Adv. Composite Mater., Vol. 16, No. 1, pp. 63–81 (2007)

Also available online - www.brill.nl/acm

Electro-elastic analysis of piezoelectric laminated plates

MINGHAO ZHAO [1], CAIFU QIAN [1], S. W. R. LEE [1], PIN TONG [1], H. SUEMASU [2] and TONG-YI ZHANG [1,*]

[1] *Department of Mechanical Engineering, Hong Kong University of Science and Technology, Clear Water Bay, Kowloon, Hong Kong, China*
[2] *Department of Mechanical Engineering, Sophia University, Tokyo, Japan*

Received 11 November 2005; accepted 20 March 2006

Abstract—Based on the Kirchhoff hypothesis of normal-remain-normal, the present work analyses piezoelectric laminated plates, wherein poled piezoelectric laminae are transversely isotropic and function as actuators. A quadric electric field is induced inside a piezoelectric lamina under a given applied voltage and mechanical bending. The governing equations for the piezoelectric laminated plate derived from the principle of virtual work in terms of the electric enthalpy have the same forms as those for a conventional composite laminated plate. We use rectangular sandwich plates of Al/PZT/Al and PZT/Al/PZT with four simply supported edges to demonstrate the prediction of the maximum bending stress in the PZT layer. The analytic solutions are verified by three-dimensional finite element analysis.

Keywords: Piezoelectric material; piezoelectric laminated plate; plate bending.

1. INTRODUCTION

Actuators and sensors made of piezoelectric materials are widely used in smart structures and systems. One kind of smart structures and systems is multilayer plates, which take advantage of the integrated properties of each layer [1–5]. Therefore, analysis of a piezoelectric laminated plate is of theoretical significance and engineering importance, and thus attracts many researchers [6–12].

There are a number of two-dimensional bending models for piezoelectric laminated plates [6–12]. Most of the models focus on the vibration properties of the piezoelectric laminated plates because of their practical importance. Tiersten's work [13] gave much of the necessary theoretical foundation for the static and dynamic behavior of a single-layer piezoelectric plate. Parton and Kudryavtsev [8] considered the general case of two-dimensional version of three-dimensional electroelastic

*To whom correspondence should be addressed. E-mail: mezhangt@ust.hk

problems in piezoelectric plates and their solutions consist of eight coupled-partial-differential equations. Mindlin [7] derived two-dimensional equations of motion for piezoelectric plates from three-dimensional equations of linear piezoelectricity by expansion in power series in the thickness coordinates of the plate. Based on the Kirchhoff plate theory, Lee and Moon [14], Lee [15], and Lee *et al*. [16] derived simple formulas for bending and torsional control. Mitchell and Reddy [9] proposed a refined hybrid plate theory of piezoelectric laminated plates. In the hybrid theory an equivalent single-layer theory is used for the mechanical displacement field, whereas the potential function for piezoelectric laminae is modeled using a layerwise discretization in the thickness direction, equivalent to modeling the variation of electric potential through the thickness with one-dimensional finite elements [9]. The hybrid model is able to analyze multilayer smart structures to accommodate multiple voltage inputs and/or sensor outputs. Heyliger [11] derived exact solutions for simply supported laminated piezoelectric plates, directly from three-dimensional governing equations without any assumptions on the variations of displacements and electric potential through the thickness. Lazarus and Crawley [17] developed pin-force and consistent plate models for the design of induced strain actuators. Dimitriadis *et al.* [18] and Wang *et al.* [19] proposed a two-dimensional model for rectangular plates to represent the behavior induced by piezoelectric patches bonded to the bottom and top surfaces of a laminate. Ray *et al.* [20] studied the behavior of an elastic layer bonded to a piezoelectric layer on the assumption that the through-thickness piezoelectric coefficient was zero. This constraint results in solutions of significant difference from those where this constant is included [21]. Sze *et al*. [22] studied two assumptions on the spatial distributions of the electric variables. One assumption is that the transverse electric field is piecewise linear along the transverse direction, and the other is that the transverse electric displacement is piecewise constant along the transverse direction. They conducted numerical calculations on laminated piezoelectric beams to demonstrate the appropriate application conditions of the two assumptions [22]. Without using any simplified assumptions, Shodja and Kamali [23] obtained an accurate three-dimensional solution in series. For practice, however, it might be more desirable to use simple analytic solutions with sufficient accuracy. Simple analytic solutions are usually derived from modeling based on certain assumptions, and therefore they are appropriate in certain aspects of applications.

When considering the deflection of a piezoelectric composite beam or plate under an applied electric field, the Infinite-Plane-Capacitor (IPC) assumption is frequently used in the literature to develop simplified models for piezoelectric layers whose two surfaces are fully electroded [6, 10, 12]. The IPC assumption means that the electric field strength inside a piezoelectric lamina under a given applied voltage is constant and independent of the in-plane coordinates. Thus, it reduces problems for piezoelectric laminated plates to the conventional plate problems and hence substantially simplifies the solution procedure. The simplified solutions based on the IPC assumption predict, to a large extent, the flexural-extensional vibration

behavior [6, 10, 12, 15]. In the present work, we show that the electric field can be approximately linear in the piezoelectric lamina when the piezoelectric composite plate is under combined mechanical and electrical loading. This linear electric field is then subjected to high stresses in the piezoelectric lamina, which are essential in designs when reliability is a major concern.

2. ANALYSIS

2.1. Displacements and strains in a laminated plate

Figure 1 shows schematically a general (N+M)-layered piezoelectric laminated plate with M piezoelectric laminae and N non-piezoelectric laminae. The piezoelectric laminae are transversely isotropic, with all the planes of isotropy being parallel to the surfaces of the laminae, and their poling direction is in the thickness direction. The two surfaces of each PZT lamina are fully electroded. The Cartesian coordinate system is used with its z-axis along the thickness direction of the plate. We use z_k and z_{k-1} to denote the two surfaces of the kth layer.

In this paper, the following assumptions are made:

(1) perfect bonding at all interfaces;

(2) a zero value of the stress component σ_z;

(3) validity of the Kirchhoff hypothesis of normal-remain-normal;

(4) no in-plane electric components of E_x and E_y; and

(5) no electric fields in the non-piezoelectric laminae.

According to the Kirchhoff hypothesis, the displacements of the plate can be expressed as follows [22, 23]:

$$\begin{aligned} u(x, y, z) &= u^0(x, y) - z w_{,x}, \\ v(x, y, z) &= v^0(x, y) - z w_{,y}, \\ w(x, y, z) &= w(x, y), \end{aligned} \tag{1}$$

where $u^0(x, y)$ and $v^0(x, y)$ are the in-plane displacements, $w(x, y)$ is the out-plane deflection of the middle-surface, thereafter, a comma "," in the subscript denotes differentiation with respect to the following coordinate(s). From equation (1), we have the strain fields

$$\begin{aligned} &\varepsilon_x = \varepsilon_x^0 + z k_x, \quad \varepsilon_y = \varepsilon_y^0 + z k_y, \\ &\gamma_{xy} = \gamma_{xy}^0 + z k_{xy}, \\ &\gamma_{xz} = 0, \quad \gamma_{yz} = 0, \end{aligned} \tag{2}$$

where

$$\begin{aligned} &\varepsilon_x^0 = u_{,x}^0, \quad \varepsilon_y^0 = v_{,y}^0, \quad \gamma_{xy}^0 = u_{,y}^0 + v_{,x}^0, \\ &k_x = -w_{,xx}, \quad k_y = -w_{,yy}, \quad k_{xy} = -2w_{,xy}. \end{aligned} \tag{3}$$

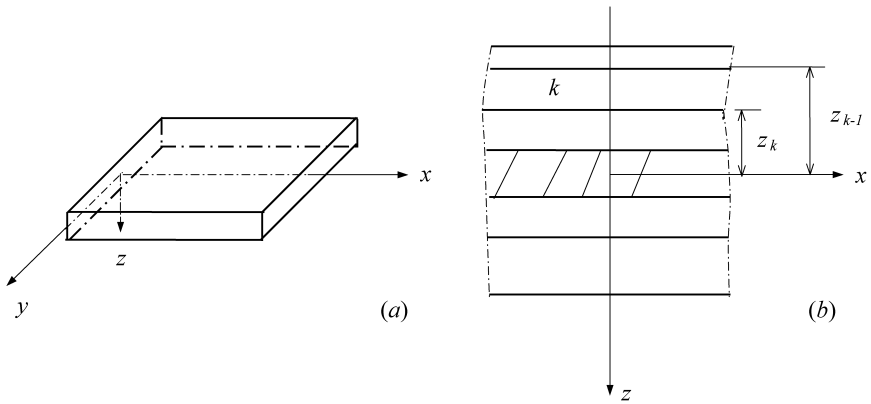

Figure 1. (N+M)-layered piezoelectric laminated plate of N non-piezoelectric laminae and M piezoelectric laminae.

2.2. Lamina constitutive relationship

The linear constitutive equations for a PZT lamina are given by [8]

$$\begin{bmatrix} \sigma_x \\ \sigma_y \\ \sigma_z \\ \tau_{yz} \\ \tau_{xz} \\ \tau_{xy} \end{bmatrix} = \begin{bmatrix} c_{11}^p & c_{12}^p & c_{13}^p & 0 & 0 & 0 \\ c_{12}^p & c_{11}^p & c_{13}^p & 0 & 0 & 0 \\ c_{13}^p & c_{13}^p & c_{33}^p & 0 & 0 & 0 \\ 0 & 0 & 0 & c_{44}^p & 0 & 0 \\ 0 & 0 & 0 & 0 & c_{44}^p & 0 \\ 0 & 0 & 0 & 0 & 0 & c_{66}^p \end{bmatrix} \begin{bmatrix} \varepsilon_x \\ \varepsilon_y \\ \varepsilon_z \\ \gamma_{yz} \\ \gamma_{xz} \\ \gamma_{xy} \end{bmatrix} - \begin{bmatrix} 0 & 0 & e_{31} \\ 0 & 0 & e_{31} \\ 0 & 0 & e_{33} \\ 0 & e_{15} & 0 \\ e_{15} & 0 & 0 \\ 0 & 0 & 0 \end{bmatrix} \begin{bmatrix} E_x \\ E_y \\ E_z \end{bmatrix}, \tag{4}$$

$$\begin{bmatrix} D_x \\ D_y \\ D_z \end{bmatrix} = \begin{bmatrix} 0 & 0 & 0 & 0 & e_{15} & 0 \\ 0 & 0 & 0 & e_{15} & 0 & 0 \\ e_{31} & e_{31} & e_{33} & 0 & 0 & 0 \end{bmatrix} \begin{bmatrix} \varepsilon_x \\ \varepsilon_y \\ \varepsilon_z \\ \gamma_{yz} \\ \gamma_{xz} \\ \gamma_{xy} \end{bmatrix} + \begin{bmatrix} \varepsilon_{11} & 0 & 0 \\ 0 & \varepsilon_{11} & 0 \\ 0 & 0 & \varepsilon_{33} \end{bmatrix} \begin{bmatrix} E_x \\ E_y \\ E_z \end{bmatrix}, \tag{5}$$

where $\sigma_x, \cdot\cdot, \varepsilon_x, \cdot\cdot, \cdot\cdot, D_x, \cdot\cdot$ and $E_x, \cdot\cdot$ are the components of the stress, strain, electric displacement and the electric field, respectively, and c_{ij}^p, e_{ij} and ε_{ij} are the elastic, piezoelectric and dielectric constants, respectively. Following assumption (2)

and from equation (4), we obtain [8]

$$\varepsilon_z = -\frac{c_{13}^p}{c_{33}^p}(\varepsilon_x + \varepsilon_y) + \frac{e_{33}}{c_{33}^p}E_z. \tag{6}$$

A substitution of equations (2) and (6) into equations (4) and (5) yields

$$\begin{aligned}\begin{bmatrix}\sigma_x\\ \sigma_y\\ \tau_{xy}\end{bmatrix} &= \begin{bmatrix}Q_{11}^p & Q_{12}^p & 0\\ Q_{12}^p & Q_{11}^p & 0\\ 0 & 0 & Q_{66}^p\end{bmatrix}\begin{bmatrix}\varepsilon_x\\ \varepsilon_y\\ \gamma_{xy}\end{bmatrix} - \begin{bmatrix}0 & 0 & e_{31}^p\\ 0 & 0 & e_{31}^p\\ 0 & 0 & 0\end{bmatrix}\begin{bmatrix}E_x\\ E_y\\ E_z\end{bmatrix}\\ &\equiv \left[Q^p\right]\begin{bmatrix}\varepsilon_x\\ \varepsilon_y\\ \gamma_{xy}\end{bmatrix} - \left[e^p\right]\begin{bmatrix}E_x\\ E_y\\ E_z\end{bmatrix},\end{aligned} \tag{7}$$

$$\begin{bmatrix}D_x\\ D_y\\ D_z\end{bmatrix} = \left[e^p\right]^T\begin{bmatrix}\varepsilon_x\\ \varepsilon_y\\ \gamma_{xy}\end{bmatrix} + \begin{bmatrix}\varepsilon_{11} & 0 & 0\\ 0 & \varepsilon_{11} & 0\\ 0 & 0 & \varepsilon_{33}^p\end{bmatrix}\begin{bmatrix}E_x\\ E_y\\ E_z\end{bmatrix}, \tag{8}$$

where the reduced elastic, piezoelectric and dielectric constants are given by

$$\begin{aligned}Q_{ij}^p &= c_{ij}^p - \frac{c_{i3}^p c_{j3}^p}{c_{33}^p}, \quad i, j = 1, 2, 6,\\ e_{31}^p &= e_{31} - \frac{c_{13}^p}{c_{33}^p}e_{33}, \quad \varepsilon_{33}^p = \varepsilon_{33} + \frac{e_{33}^2}{c_{33}^p}.\end{aligned} \tag{9}$$

For comparison, we briefly describe the Infinite-Plane-Capacitor (IPC) assumption. The IPC hypothesis assumes that the electric field is the same as that in an infinite plane capacitor [6, 10, 12, 15] such that the potential in the PZT lamina could be expressed in the form of

$$\varphi(x, y, z) = \varphi^0 + z\psi, \tag{10a}$$

where φ^0 is a reference electrical potential and ψ is a constant representing the potential gradient through thickness. Equation (10a) is equivalent to

$$E_x = 0, \quad E_y = 0, \quad -E_z = -E_z^0 = \frac{V}{t_p}, \tag{10b}$$

where E_z^0 is the apparent electric field strength, and V and t_p are the applied electric voltage between the two electrodes and the thickness of the PZT layer, respectively. Due to the piezoelectric effect, an external mechanical load, in addition to the loading of electric voltage, induces an electric field which generally differs from that given by equation (10a) or (10b). In return, the electric field induced by both electric and mechanical loading produce a mechanical field, which is essential and important to reliability designs. To account for this coupling effect, we introduce assumption (4) to replace the IPC assumption and accordingly derive the electric

field from equation (8). Using the dielectric governing equation

$$D_{x,x} + D_{y,y} + D_{z,z} = 0, \tag{11}$$

together with equations (2) and (8) and assumption (4), we have

$$e_{31}^{p}(k_x + k_y) - \varepsilon_{33}^{p}\varphi_{,zz} = 0. \tag{12}$$

The general solution of equation (12) is

$$\varphi = \frac{e_{31}^{p}}{\varepsilon_{33}^{p}}\frac{z^2}{2}(k_x + k_y) + z\varphi_1 + \varphi_2, \tag{13}$$

where φ_1 and φ_2 are two unknown functions of x and y. If an electric potential voltage V is applied between the two electrodes, φ_1 and φ_2 can be determined and equation (13) has the form of

$$\varphi = -E_z^0(z - z_0) + \frac{1}{2}\frac{e_{31}^{p}}{\varepsilon_{33}^{p}}(k_x + k_y)(z - z_u)(z - z_l) + \frac{1}{2}(\varphi_u + \varphi_l), \tag{14}$$

where z_u and z_l are the z-coordinates of the two surfaces of the corresponding piezoelectric lamina, and φ_u and φ_l are the electric potentials on these two surfaces. Similar results were obtained in piezoelectric beam [24] and thin shell analyses [8]. Consequently, differentiating equation (14) with respect to z leads to the electric field strength

$$E_z = E_z^0 - \frac{e_{31}^{p}}{\varepsilon_{33}^{p}}(k_x + k_y)(z - z_0), \tag{15}$$

where $z_0 = (z_u + z_l)/2$. As indicated in equation (15), the electric field varies linearly through the thickness of the PZT lamina. Substituting equation (15) into constitutive equations (7) and (8) and considering assumption (4), we have the modified reduced constitutive equations for the piezoelectric lamina:

$$\begin{bmatrix} \sigma_x \\ \sigma_y \\ \tau_{xy} \end{bmatrix} = [Q^p] \begin{bmatrix} \varepsilon_x^0 \\ \varepsilon_y^0 \\ \gamma_{xy}^0 \end{bmatrix} + \left(z[Q^p] + (z - z_0)[Q^{pp}]\right) \begin{bmatrix} k_x \\ k_y \\ k_{zy} \end{bmatrix} - \begin{bmatrix} e_{31}^{p} \\ e_{31}^{p} \\ 0 \end{bmatrix} E_z^0, \tag{16}$$

$$D_z = \varepsilon_{33}^{p} E_z^0 + e_{31}^{p}(\varepsilon_x^0 + \varepsilon_y^0) + e_{31}^{p}(k_x + k_y)z_0, \tag{17}$$

where

$$[Q^{pp}] = \begin{bmatrix} (e_{31}^{p})^2/\varepsilon_{33}^{p} & (e_{31}^{p})^2/\varepsilon_{33}^{p} & 0 \\ (e_{31}^{p})^2/\varepsilon_{33}^{p} & (e_{31}^{p})^2/\varepsilon_{33}^{p} & 0 \\ 0 & 0 & 0 \end{bmatrix}, \tag{18}$$

$[Q^{pp}]$ is the modified reduced stiffness matrix. In equations (16) and (17) strains and electric field strengths are expressed in terms of the midplane strains, the curvatures and the apparent electric field strength. Under a given applied electric voltage, the apparent electric field strength is a constant for a fixed PZT lamina thickness. On

the right-hand side of equation (16), the first term gives the stress field due to the middle-surface stretching, the third term represents the reverse piezoelectric effect, and the second term is the bending stress. The bending stresses are related not only to the reduced stiffness matrix, but also to the modified reduced stiffness matrix, equation (18), which will change the bending stresses significantly. Neglecting the modified reduced stiffness matrix $[Q^{pp}]$ reduces equation (16) to the constitutive equation based on the IPC assumption.

We assume that non-piezoelectric laminas are orthotropic and hence have the reduced constitute equations [24, 25]

$$\begin{bmatrix} \sigma_x \\ \sigma_y \\ \tau_{xy} \end{bmatrix} = \begin{bmatrix} Q_{11}^g & Q_{12}^g & Q_{16}^g \\ Q_{12}^g & Q_{22}^g & Q_{26}^g \\ Q_{16}^g & Q_{26}^g & Q_{66}^g \end{bmatrix} \begin{bmatrix} \varepsilon_x \\ \varepsilon_y \\ \gamma_{xy} \end{bmatrix} = \left[Q^g\right] \begin{bmatrix} \varepsilon_x \\ \varepsilon_y \\ \gamma_{xy} \end{bmatrix}, \tag{19}$$

where

$$[Q^g] = [T]^{-1}[Q][T]^{-\mathrm{T}}, \tag{20}$$

and

$$[T] = \begin{bmatrix} \cos^2\theta & \sin^2\theta & 2\sin\theta\cos\theta \\ \sin^2\theta & \cos^2\theta & -2\sin\theta\cos\theta \\ -\sin\theta\cos\theta & \sin\theta\cos\theta & \cos^2\theta - \sin^2\theta \end{bmatrix}, \tag{21}$$

with θ being the angle from the x-axis to the first principal material coordinates [24, 25]. The elements of the matrix $[Q]$ are determined from the stiffness matrix

$$Q_{ij} = c_{ij} - \frac{c_{i3}c_{3j}}{c_{33}}, \quad i, j = 1, 2, 6. \tag{22}$$

2.3. Laminate constitutive equations

The stress resultants and moment for a plate are defined as [24, 25]

$$\begin{bmatrix} N_x \\ N_y \\ N_{xy} \end{bmatrix} = \int \begin{bmatrix} \sigma_x \\ \sigma_y \\ \tau_{xy} \end{bmatrix} \mathrm{d}z, \quad \begin{bmatrix} M_x \\ M_y \\ M_{xy} \end{bmatrix} = \int \begin{bmatrix} \sigma_x \\ \sigma_y \\ \tau_{xy} \end{bmatrix} z\,\mathrm{d}z. \tag{23}$$

Substituting equations (16) and (19) into (23) yields the constitute equations of the piezoelectric laminated plate

$$\begin{bmatrix} N_x \\ N_y \\ N_{xy} \\ M_x \\ M_y \\ M_{xy} \end{bmatrix} = \begin{bmatrix} A & B \\ B & D \end{bmatrix} \begin{bmatrix} \varepsilon_x^0 \\ \varepsilon_y^0 \\ \varepsilon_{xy}^0 \\ k_x \\ k_y \\ k_{xy} \end{bmatrix} - \begin{bmatrix} N_{x0} \\ N_{y0} \\ N_{xy0} \\ M_{x0} \\ M_{y0} \\ M_{xy0} \end{bmatrix}, \tag{24}$$

where the elements of the matrices are

$$
\begin{aligned}
A_{ij} &= \sum_{n=1}^{N} \left(Q_{ij}^{g}\right)_n (z_n - z_{n-1}) + \sum_{m=1}^{M} \left(Q_{ij}^{P}\right)_m (z_m - z_{m-1}), \\
B_{ij} &= \frac{1}{2} \sum_{n=1}^{N} \left(Q_{ij}^{g}\right)_n (z_n^2 - z_{n-1}^2) + \frac{1}{2} \sum_{m=1}^{M} \left(Q_{ij}^{p}\right)_m (z_m^2 - z_{m-1}^2), \\
C_{ij} &= B_{ij}, \qquad\qquad i, j = 1, 2, 6 \\
D_{ij} &= \frac{1}{3} \sum_{n=1}^{N} \left(Q_{ij}^{g}\right)_n (z_n^3 - z_{n-1}^3) \\
&\quad + \frac{1}{3} \sum_{m=1}^{M} \left[\left(Q_{ij}^{p}\right)_m (z_m^3 - z_{m-1}^3) + \frac{1}{4} \left(Q_{ij}^{pp}\right)_m (z_m - z_{m-1})^3 \right],
\end{aligned}
\tag{25}
$$

$$
\begin{aligned}
N_{x0} &= \sum_{m=1}^{M} \left(e_{31} E_z^0\right)_m (z_m - z_{m-1}), \quad N_{y0} = N_{x0},\ N_{xy0} = 0, \\
M_{x0} &= \frac{1}{2} \sum_{m=1}^{M} \left(e_{31} E_z^0\right)_m (z_m^2 - z_{m-1}^2), \quad M_{y0} = M_{x0},\ M_{xy0} = 0.
\end{aligned}
\tag{26}
$$

In equations (24) and (25), the A_{ij} are extensional stiffnesses, the B_{ij} are bending-extension coupling stiffnesses, and the D_{ij} are bending stiffnesses. For convenience, equation (24) is rewritten in a compact form

$$
\begin{bmatrix} N \\ M \end{bmatrix} = \begin{bmatrix} A & B \\ B & D \end{bmatrix} \begin{bmatrix} \varepsilon^0 \\ k \end{bmatrix} - \begin{bmatrix} N_0 \\ M_0 \end{bmatrix}. \tag{27}
$$

Equations (25) and (26) show that the stiffnesses A_{ij} and B_{ij} in the present model are identical to those in the IPC model, but the bending stiffness D_{ij} are different in the two models due to the modified reduced stiffness Q_{ij}^{pp}.

2.4. Governing equations of laminated piezoelectric plate

The governing equations for piezoelectric plate are formulated from the principle of virtual work [8, 27]

$$
\delta P_H = \delta H - \delta W = \int_{\Pi} \delta h \, \mathrm{d}\Pi - \int_{\Gamma} (t_i \delta u_i + D_i n_i \delta\varphi) \, \mathrm{d}\Gamma = 0, \tag{28}
$$

where Π and Γ denote, respectively, the entire domain and domain boundaries, t_i are the tractions, and n_i are the components of the unit outward normal to Γ. It should be kept in mind that in equation (28), the variables are strains and electric field strengths and further displacements and electric potential, u^0, v^0, w, and E_z^0.

The total electric enthalpy for the entire domain is given by

$$H = \int \frac{1}{2}\left\{\int [\sigma_{ij}\varepsilon_{ij} - D_i E_i]\,\mathrm{d}z\right\}\mathrm{d}x\,\mathrm{d}y. \tag{29}$$

Substituting equations (15-17) and (19) into (29) and using (24), we obtain

$$\begin{aligned} H = \frac{1}{2}\int \big\{&[\varepsilon^0]^{\mathrm{T}}[A][\varepsilon^0] + 2[\varepsilon^0]^{\mathrm{T}}[B][k] + [k]^{\mathrm{T}}[D][k] \\ &- 2[N_0]^{\mathrm{T}}[\varepsilon^0] - 2[M_0]^{\mathrm{T}}[k] - h_0\big\}\,\mathrm{d}x\,\mathrm{d}y, \end{aligned} \tag{30}$$

where

$$\begin{aligned} h_0 &= \sum_{m=1}^{M}\left[\varepsilon_{33}^p (E_z^0)^2 + E_z^0[e_{31}^p(\varepsilon_x^0 + \varepsilon_y^0) + e_{31}^p(k_x + k_y)z_0]\right]_m (z_m - z_{m-1}) \\ &\approx \sum_{m=1}^{M}\left[\varepsilon_{33}^p (E_z^0)^2\right]_m (z_m - z_{m-1}). \end{aligned}$$

Note that the coupling term in h_0 is approximately ignored for simplicity. Since the apparent electric field strength depends only on the applied voltage and the thickness of the PZT lamina, the variation of equation (30) yields

$$\begin{aligned} \delta H = \int \big\{&\big([\varepsilon^0]^{\mathrm{T}}[A] + [k]^{\mathrm{T}}[B] - [N_0]^{\mathrm{T}}\big)[\delta\varepsilon^0] \\ &+ \big([\varepsilon^0]^{\mathrm{T}}[B] + [k]^{\mathrm{T}}[D] - [M_0]^{\mathrm{T}}\big)[\delta k]\big\}\,\mathrm{d}x\,\mathrm{d}y. \end{aligned} \tag{31}$$

The displacements and the deflection are chosen to satisfy the prescribed displacement boundary values, i.e. the variations of displacement and deflection are zero at the portion of the edge on which the displacements and deflection are prescribed. Under lateral mechanical loading, i.e. prescribed forces at the plate edges, s_{xf} and s_{yf}, and given electric voltages, we have

$$\begin{aligned} \delta W = &\int q\delta w\,\mathrm{d}x\,\mathrm{d}y + \int_{s_{xf}} (\overline{N}_x\delta u + \overline{N}_{xy}\delta v - \overline{M}_x\delta w_{,x} + \overline{V}_x\delta w)\,\mathrm{d}s \\ &+ \int_{s_{yf}} (\overline{N}_{xy}\delta u + \overline{N}_y\delta v - \overline{M}_y\delta w_{,y} + \overline{V}_y\delta w)\,\mathrm{d}s, \end{aligned} \tag{32}$$

where q is the applied load distribution. s_{xf} is defined along the edges $x =$ constant and s_{yf} along the edges $y =$ constant, and the over-bar denotes a "prescribed" value. Substituting of equations (31) and (32) into (28) and then using Green's theorem in conjunction with integration by parts lead to the governing equations

$$\begin{aligned} &A_{11}u^0_{,xx} + 2A_{16}u^0_{,xy} + A_{66}u^0_{,yy} + A_{16}v^0_{,xx} + (A_{12} + A_{66})v^0_{,xy} + A_{26}v^0_{,yy} \\ &\quad - B_{11}w_{,xxx} - 3B_{16}w_{,xxy} - (B_{12} + 2B_{66})w_{,xyy} - B_{26}w_{,yyy} = 0, \end{aligned} \tag{33}$$

and

$$A_{16}u^0_{,xx} + (A_{12} + A_{66})u^0_{,xy} + A_{26}u^0_{,yy} + A_{66}v^0_{,xx}\frac{\partial^2 v^0}{\partial x^2} + 2A_{26}v^0_{,xy} + A_{22}v^0_{,yy} - B_{16}w_{,xxx} - (B_{12} + 2B_{66})w_{,xxy} - 3B_{26}w_{,xyy} - B_{22}w_{,yyy} = 0, \tag{34}$$

$$\begin{aligned} &- B_{11}u^0_{,xxx} - 3B_{16}u^0_{,xxy} - (B_{12} + 2B_{66})u^0_{,xyy} - B_{26}u^0_{,yyy} \\ &- B_{16}v^0_{,xxx} - (B_{12} + 2B_{66})v^0_{,xxy} - 3B_{26}v^0_{,xyy} - B_{22}v^0_{,yyy} \\ &+ D_{11}w_{,xxxx} + 4D_{16}w_{,xxxy} + 2(D_{12} + 2D_{66})w_{,xxyy} \\ &+ 4D_{26}w_{,xyyy} + D_{22}w_{,yyyy} = q(x, y), \end{aligned} \tag{35}$$

and the force boundary conditions

$$\begin{aligned} &N_x = \bar{N}_x, \quad N_{xy} = \bar{N}_{xy} \\ &M_x = \bar{M}_x \quad M_{x,x} + 2M_{xy,y} = \bar{V}_x, \end{aligned} \quad \text{on } s_{xf}, \tag{36}$$

$$\begin{aligned} &N_{xy} = \bar{N}_{xy}, \quad N_y = \bar{N}_y, \\ &M_y = \bar{M}_y, \quad 2M_{xy,x} + M_{y,y} = \bar{V}_y \end{aligned} \quad \text{on } s_{yf}, \tag{37}$$

where N_x, M_x, ... are in terms of the displacements and the deflection by equation (24) or (27). Governing equations (33)–(35) have the same forms as those governing equations for conventional composite laminated plates [24, 25]. Therefore, equations (33)–(35) can be solved by using the available methods including the reduced bending method [24, 25, 28].

3. EXAMPLES

3.1. Analysis of Al/PZT/Al laminated plate

To demonstrate the proposed model, we first consider a rectangular sandwich plate of Al/PZT-5H/Al of $a \times b$ with $a = 0.078$ m, where a and b are the plate length and width, respectively. The thickness of the top or bottom Al lamina is $t = 1.00 \times 10^{-3}$ m and the thickness of PZT core is $t_p = 0.87 \times 10^{-3}$ m [29]. The material properties are listed in Table 1. The midplane of the PZT lamina is set to be the *Oxy* plane. In this case, the bending-extension coupling stiffnesses B_{ij} and the stiffness components D_{16} and D_{26} are all equal to zero. The edges of the rectangular are simply supported. The boundary conditions are:

$$\begin{aligned} &w = 0, \quad M_x = -D_{11}w_{,xx} - D_{12}w_{,yy} = 0 \\ &N_x = 0, \quad N_{xy} = 0 \end{aligned} \quad \text{for } x = 0 \text{ or } a, \tag{38}$$

$$\begin{aligned} &w = 0, \quad M_y = -D_{12}w_{,xx} - D_{22}w_{,yy} = 0 \\ &N_{xy} = 0, \quad N_y = 0 \end{aligned} \quad \text{for } y = b/2 \text{ or } -b/2. \tag{39}$$

Table 1.
Material properties of Al and PZT laminae (E and G in units of GPa, e in C/m^2 and ε in 10^{-9} F/m)

	E_1	E_2	E_3	G_{12}	G_{13}	ν	ε_{11}	ε_{33}	e_{33}	$-e_{31}$
Al	70.3	70.3	70.3	26.1	26.1	0.34	–	–	–	–
PZT	61	61	48	23.3	19.1	0.31	6.0	6.0	21.319	14.645

In this case, the in-plane solution is trivial, i.e. $u^0 = v^0 = 0$ and the deflection governing equation is simplified to

$$D_{11}w_{,xxxx} + 2(D_{12} + 2D_{66})w_{,xxyy} + D_{22}w_{,yyyy} = q(x, y). \tag{40}$$

If the applied electric voltage $V = 0$ and the transverse load is uniformly distributed along $x = a/2$ that

$$q(x, y) = \delta\left(x - \frac{a}{2}\right)q_0, \tag{41}$$

where δ is the Dirac Delta function and $q_0 = 1.0 \times 10^{-3}$ N/m, equations (38)–(40) are solved by the well-known Levy method [24, 25]. The deflection is given by

$$w = \sum_{m=1,3,\ldots}^{\infty}\left[\sum_{i=1}^{4} F_{im}\mathrm{e}^{\lambda_i \frac{m\pi}{a} y} - F_m\right]\sin\left(\frac{m\pi x}{a}\right), \tag{42}$$

where

$$\begin{aligned}
\lambda_1 &= \frac{D_{12} + 2D_{66} - \sqrt{(D_{12} + 2D_{66})^2 - D_{11}D_{22}}}{D_{11}}, \quad \lambda_3 = -\lambda_1, \\
\lambda_2 &= \frac{D_{12} + 2D_{66} + \sqrt{(D_{12} + 2D_{66})^2 - D_{11}D_{22}}}{D_{11}}, \quad \lambda_4 = -\lambda_2, \\
F_m &= -\frac{2q_0}{aD_{11}(m\pi/a)^4}\sin\left(\frac{m\pi}{2}\right),
\end{aligned} \tag{43}$$

and the coefficients F_{im} are determined by the following algebraic equations:

$$\begin{aligned}
&\sum_{i=1}^{4} F_{im}\mathrm{e}^{r_m\lambda_i} = F_m, \\
&\sum_{i=1}^{4} F_{im}\mathrm{e}^{-r_m\lambda_i} = F_m, \\
&\sum_{i=1}^{4} F_{im}\left(D_{12} - D_{22}\lambda_i^2\right)\mathrm{e}^{r_m\lambda_i} = D_{12}F_m, \\
&\sum_{i=1}^{4} F_{im}\left(D_{12} - D_{22}\lambda_i^2\right)\mathrm{e}^{-r_m\lambda_i} = D_{12}F_m,
\end{aligned} \qquad m = 1, 3, \ldots \tag{44}$$

in which

$$r_m = \frac{m\pi b}{2a}. \tag{45}$$

At the typical point of $x = a/2$, $y = 0$ and $z = t_p/2$ in the PZT lamina, the normalized deflection α and the normalized bending stress β at this typical point in the PZT lamina

$$\alpha = w \Big/ \frac{q_0 a^3}{D_{11}^p} = \sum_{m=1,3,\ldots}^{\infty} \left[\sum_{i=1}^{4} F_{im} - F_m \right] \sin\left(\frac{m\pi}{2}\right) \Big/ \frac{q_0 a^3}{D_{11}^p}, \tag{46}$$

$$\beta = \sigma_x \Big/ \frac{q_0 a}{t_p^2} = \left\{ \frac{t_p^3}{2q_0 a^3} \sum_{i=1}^{4} F_{im} \left[\left(Q_{11}^p + Q_{11}^{pp}\right) - \lambda_i^2 \left(Q_{12}^p + Q_{12}^{pp}\right) \right] + \frac{(Q_{11}^p + Q_{11}^{pp}) t_p^3}{D_{11}(m\pi)^4} \sin\left(\frac{m\pi}{2}\right) \right\} (m\pi)^2 \sin\left(\frac{m\pi}{2}\right), \tag{47}$$

where $D_{11}^p = E_{11}^p (t_p)^3/(12(1-\nu^2))$, in which E_{11}^p is the elastic constants of the PZT layer listed in Table 1. The normalized bending stress β and the normalized deflection α are displayed in Figs 2(a) and 2(b), respectively, as functions of the aspect ratio b/a. Figure 3 displays the bending stress in the PZT layer along the z-direction at the center point of $x = a/2$, $y = 0$ and $z = t_p/2$. The corresponding results based on the IPC assumption are also shown for comparison. Figure 2(a) and Fig. 3 show that the normalized bending stress calculated from the present model could be twice larger than that calculated from the IPC model. It is interesting to note that the values of the deflection obtained by the two models are almost the same in this case. We verify the present model using finite element analysis (FEA) with the commercial software ABAQUS. Three-dimensional 20-node solid brick elements are employed and two elements are used through the thickness of each layer of the lamina. The mesh was refined to check the accuracy and the final one comprises 1200 elements. It can be seen that the FEA results agree well with those by the present analytical method.

Because the PZT layer is sandwiched by two Al laminae, the bending stiffness is mainly from the two Al layers. In this case, though the PZT lamina is stiffened due to the modified reduced stiffness matrix $[Q^{pp}]$, as shown in equation (16), the bending stiffness is almost the same as those of the IPC model, as listed in Table 2. Therefore, there is little difference in deflection but large difference in the stress in the PZT core.

For the PZT sandwich plate, the thinner are the two Al layers, the more contribution there is from the PZT layer to the bending stiffness. Consequently, the difference between the deflections calculated by the two models will greater. Table 3 lists the ratio of the deflection calculated by the IPC model to that by the present model. The larger the ratio t_p/t of the PZT layer thickness to the Al layer

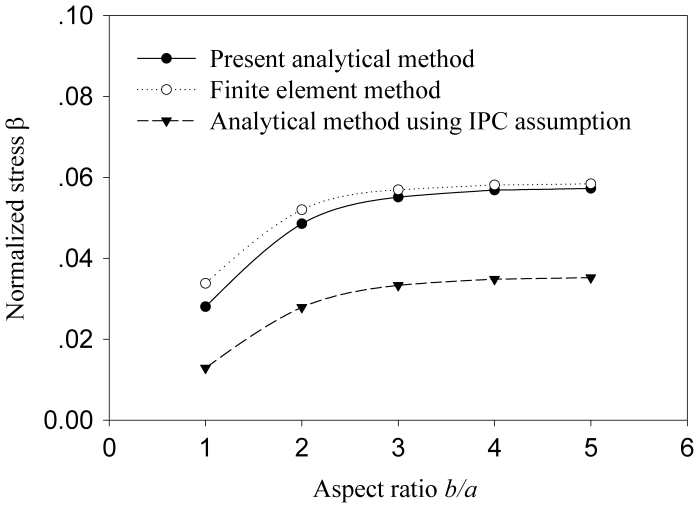

(a)

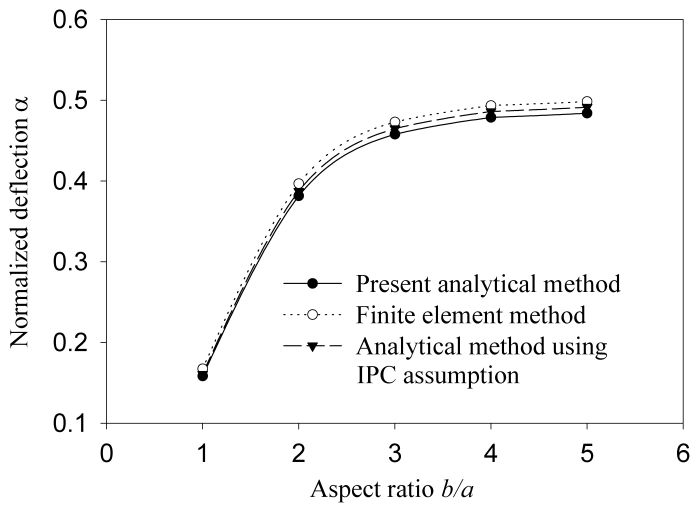

(b)

Figure 2. (a) Normalized bending stress β at the plate center $x = a/2, b = 0, z = t_p/2$ (Al/PZT/Al plate, $a = 0.078$ m, $t_p = 0.87 \times 10^{-3}$ m, $t = 1.00 \times 10^{-3}$ m). (b) Normalized deflection α at the plate center (Al/PZT/Al plate, where $a = 0.078$ m, $t_p = 0.87 \times 10^{-3}$ m, $t = 1.00 \times 10^{-3}$ m).

thickness, the larger the deflection ratio and the closer to unity is the stress ratio. For the thickness ratio of $t_p/t = 1$, the stress and deflection ratios are respectively 0.608 and 1.021, indicating that the stresses calculated by the two models differ greatly, while the deflections are almost the same. For $t_p/t = 100$, however, the stress ratio is 0.986, while the deflection ratio is 1.654. This is because when the thickness of Al layers is equal to zero, the laminated plate reduces to a pure piezoelectric plate. For a homogenous, transversely isotropic plate, the stress is independent

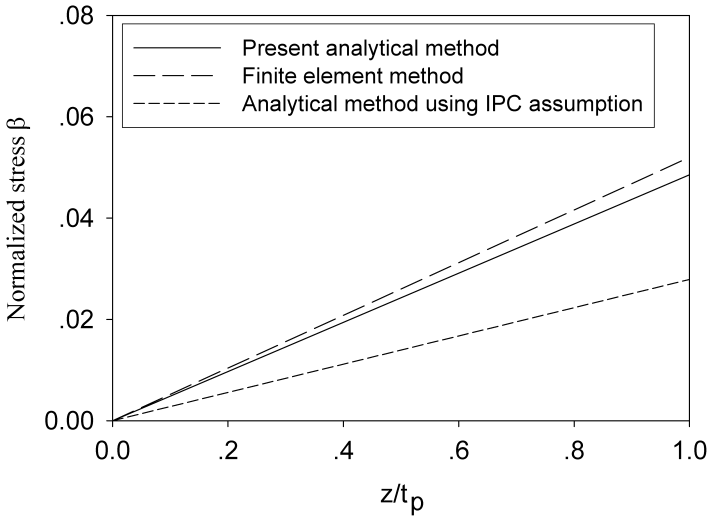

Figure 3. Normalized bending stress β along the z-direction at the plate center $x = a/2, b = 0$, $z = t_p/2$ (Al/PZT/Al plate, $a = 0.078$ m, $b/a = 2.0$, $t_p = 0.87 \times 10^{-3}$ m, $t = 1.00 \times 10^{-3}$ m).

Table 2.
The stiffnesses and characteristic roots of the Al/PZT/Al plate ($t = 1.0\times10^{-3}$ m, $t_p = 0.87\times10^{-3}$ m) $\lambda_1 = \lambda, \lambda_2 = -\lambda, \lambda_3 = \bar{\lambda}, \lambda_4 = -\bar{\lambda}, I = \sqrt{-1}$

	D_{11}	D_{12}	D_{22}	D_{66}	λ
Present model	158.930	53.9796	158.930	51.2896	$0.996264 + 0.0863653I$
IPC model	156.5260	51.5757	156.5260	51.2896	$0.996206 + 0.0870259I$

Table 3.
Comparison of bending stress in the PZT layer and center deflection calculated form the two models (Al/PZT/Al plate, $a = 0.078$ m, $b/a = 3$, $t_p = 0.87 \times 10^{-3}$ m, $q_0 = 1.0 \times 10^{-3}$ N/m) $R_S = (\sigma_{x\,\max})_{\text{IPC}}/(\sigma_{x\,\max})_{\text{Present}}$, $R_w = (w)_{\text{IPC}}/(w)_{\text{Present}}$

t_p/t	1.0	10.0	20.0	40.0	50.0	60.0	70.0	80.0	90.0	100.0
R_S	0.608	0.814	0.892	0.946	0.959	0.968	0.974	0.979	0.983	0.986
R_w	1.021	1.366	1.496	1.554	1.608	1.623	1.634	1.642	1.649	1.654

of the material properties, because the influence of Poisson's ratio is very small for general materials, as shown in equation (47), whereas the deflection depends greatly on the bending stiffness.

Next, we consider the Al/PZT/Al plate subjected only to electric loading, i.e. an electric voltage is given between the two electrodes. From the governing equations and the boundary conditions, it is easy to show that the deflection w, the resultant forces N_x, N_y, N_{xy}, and moments M_x, M_y and M_{xy} are all equal to zero. Therefore, the stress in the PZT layer or in the Al layer is uniform. The stress in the PZT layer

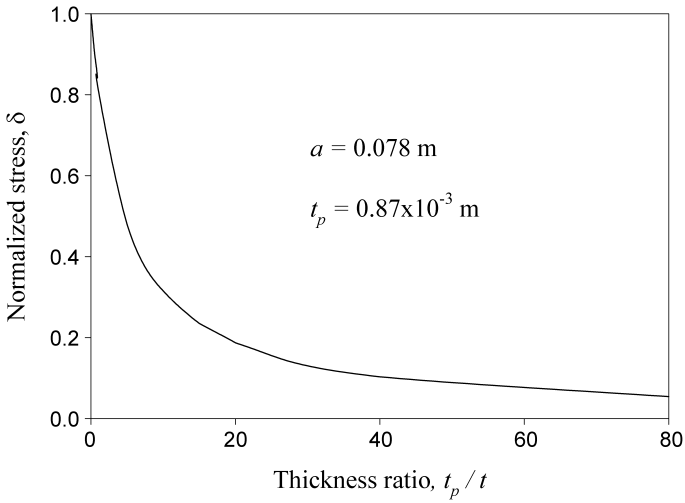

Figure 4. The normalized stress *vs.* the thickness ratio under electric loading for Al/PZT/Al plate.

is obtained as

$$[\sigma] = [Q^p][A]^{-1}[N_0] - e_{31}^p E_z^0 \begin{bmatrix} 1 \\ 1 \\ 0 \end{bmatrix}, \tag{48}$$

where $[A]$, $[Q^p]$, and $[N_0]$ are given in equations (7), (25) and (26). Figure 4 depicts the normalized stress

$$\delta = -\sigma_x / \left(e_{31}^p E_z^0\right). \tag{49}$$

It can be seen in Fig. 4 that when the thickness of the Al layer approaches zero, the stress in the PZT layer approaches zero. In this case, the laminated plate is reduced to a pure piezoelectric plate, and the PZT layer can deform freely without any constraints. When the thickness t approaches infinity, the normalized stress is equal to 1.0. It should be pointed out that in this case the solutions based on the two models are identical because of the identical stiffness A_{ij} as described in the last section. In general, solutions based on the two models are the same for problems without bending.

3.2. Analysis of PZT/Al/PZT laminated plate

As another example, we analyze the sandwich plate of PZT/Al/PZT, with two piezoelectric laminae. The loading conditions and sample parameters are the same as those in the last example. The bending stiffnesses D_{ij} and the characteristic roots are given in Table 4. Again the Levy method is used to derive the solution. The quantities $q_0 a^3 / D_{11}^p$ and $q_0 a / t_p^2$ in equations (46) and (47) are still used to normalize the deflection and stress, respectively. The maximum bending stress values σ_x at the point, $x = a/2$, $y = 0$ and $z = t/2 + t_p$, are drawn in Fig. 5. Displayed in Fig. 6 are the values of deflection. We can see that the relative error is about 20% between

Table 4.
The stiffness and characteristic roots of the PZT/Al/PZT plate ($t = 1.0\times10^{-3}$ m, $t_p = 0.87\times10^{-3}$ m) $\lambda_1 = \lambda, \lambda_2 = -\lambda, \lambda_3 = \bar{\lambda}, \lambda_4 = -\bar{\lambda}, I = \sqrt{-1}$

	D_{11}	D_{12}	D_{22}	D_{66}	λ
Present model	121.519	−27.017	121.519	40.176	$0.848204 + 0.52967I$
IPC model	116.712	−31.825	116.712	40.176	$0.841364 + 0.540469I$

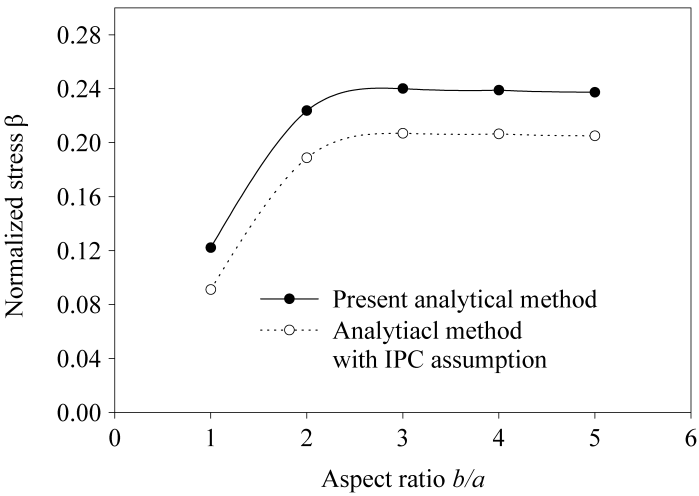

Figure 5. Normalized bending stress at the plate center $x = a/2, b = 0, z = t/2 + t_p$ (PZT/Al/PZT plate, where $a = 0.078$ m, $t_p = 0.87 \times 10^{-3}$ m, $t = 1.00 \times 10^{-3}$ m).

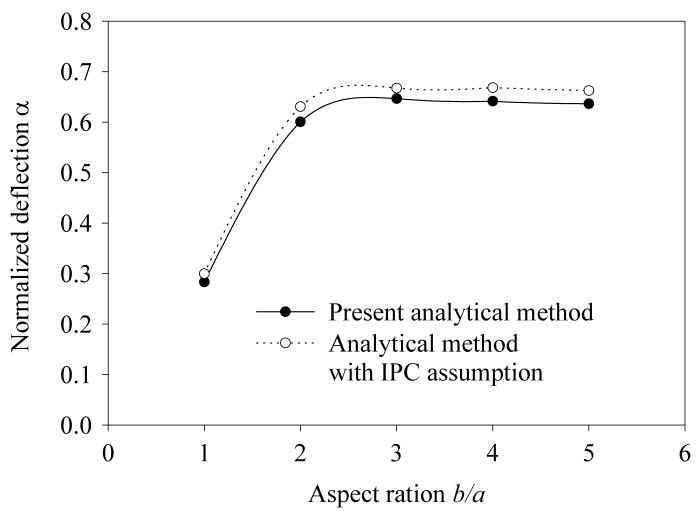

Figure 6. Normalized deflection at the plate center (PZT/Al/PZT plate, where $a = 0.078$ m, $t_p = 0.87 \times 10^{-3}$ m, $t = 1.00 \times 10^{-3}$ m).

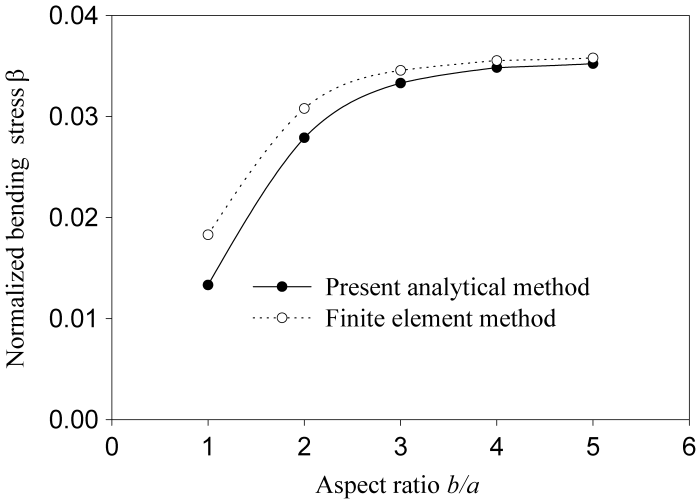

Figure 7. Comparison between the bending stresses σ_x at the center of conventional laminated plates ($a = 0.078$ m).

the stresses calculated by the present and IPC model, while the difference between the deflections is within 7%.

As shown in Fig. 2, there is some discrepancy between the analytical results and the FEM results, particularly as the aspect ratio is one. To check whether this discrepancy is induced by the piezoelectric effect, we calculate the normalized stress again using the same input data as used in plotting Fig. 2 except that the piezoelectric constants are taken to be zero. The analytic and FEM results for the conventional laminated plates are illustrated in Fig. 7. Figure 7 shows almost the same discrepancy in the normalized stress between the analytic and FEM results as that shown in Fig. 2. This means that the discrepancy is due to the approximation of the plate theory and the simplification of equation (30) rather than the quadric electric field introduced in the present work. Higher order plate theory, such as Reissner's theory [30], Mindlin's theory [31], or Reddy's theory [32], may improve the accuracy.

4. CONCLUSIONS

In the present work, we demonstrate that the electric field inside a piezoelectric lamina of a piezoelectric composite plate is dependent on the bending curvature of the plate. Therefore, the bending stiffness of the piezoelectric lamina contains the piezoelectric and dielectric parameters. The forms of the governing equation of the general piezoelectric laminated plates, derived by the principle of virtual work in terms of the in-plane displacements and the deflection, are identical to those of conventional laminated plates. As a result, the available solution method for conventional laminated plates can be used for the piezoelectric laminated plates,

including the approximated method. The results of rectangular sandwich plates, Al/PZT/Al and PZT/Al/PZT, with different aspect ratios b/a and different thickness ratio t_p/t, show that the variation of electric potential in the thickness direction must be taken into account in the structural analysis of piezoelectric laminated plates. The IPC assumption may be appropriate for cases with no bending deformation, because the piezoelectric affects primarily the bending stiffness of the PZT laminae.

Acknowledgements

This work was supported by a grant from the Research Grants Council of the Hong Kong Special Administrative Region, China. T. Y. Zhang thanks the Sophia University for the Visiting Professorship.

REFERENCES

1. H. S. Tzou and T. Fukuda, *Precision Sensors, Actuators and System,* Kluwer, Dordrecht, (1992).
2. G. H. Haerting, Rainbow ceramics – a new type of ultra high-displacement actuator, *Am. Ceram. Soc. Bull.* **73**, 93–96 (1994).
3. U. Kenji, *Piezoelectric Actuators and Ultrasonic Motors,* Kluwer Academic Publishers, Boston (1997).
4. Q. M. Wang and L. E. Cross Determination of Young's modulus of the reduced layer of a piezoelectric rainbow actuator, *J. Appl. Phys*. **83**, 5358–5363 (1998).
5. S. W. R. Lee and H. L. Li, Development and characterization of a rotary motor driven by anisotropic piezoelectric composite laminate, *Smart Mater. Struct*. **7**, 327–336 (1998).
6. N. T. Adelman and Y. Stavsky, Flexural-extensional behavior of composite piezoelectric circular plates, *J. Acoust. Soc. Amer*. **67**, 819–822 (1980).
7. R. D. Mindlin, Frequency of piezoelectrically forced vibrations of electroded, doubly rotated quartz plates, *Int. J. Solid Struct*. **20**, 141–157 (1984).
8. V. Z. Parton and B. A. Kudryavtsev, *Electromagnetoelasticity,* Gordon and Breach Science Publishers, New York (1988).
9. J. A. Mitchell and J. N. Reddy, A refined hybrid plate theory for composite laminates with piezoelectric laminate, *Int. J. Solids Struct*. **32**, 2345–2367 (1995).
10. X. D. Zhang and C. T. Sun, Formulation of an adaptive sandwich beam, *Smart Mater. Struct*. **5**, 841–823 (1996).
11. P. Heyliger, Exact solution for simply supported laminated piezoelectric plates, *J. Appl. Mech*. **64**, 299–306 (1997).
12. X. D. Zhang and C. T. Sun, Analysis of a sandwich plate containing a piezoelectric core, *Smart Mater. Struct.* **8**, 31–40 (1999).
13. H. F. Tiersten, *Linear Piezoelectric Plate Vibrations,* Plenum, New York (1969).
14. C.-K. Lee and F. C. Moon, Laminated piezopolymer plates for torsion and bending sensors and actuators, *J. Acoust. Soc. Amer*. **85**, 2432–2439 (1989).
15. C.-K. Lee, Theory of laminated plates for the design of distributed sensors/actuators Part I: Governing equation and reciprocal relations, *J. Acoust. Soc. Amer*. **87**, 1144–1158 (1990).
16. C.-K. Lee, W.-W. Chiang and T. C. O'Sullivan, Piezoelectric modal sensors/actuators pairs for critical active damping vibration control, *J. Acoust. Soc. Amer*. **90**, 374–384 (1992).
17. K. B. Lazarus and E. F. Crawley, *Induced strain actuation of composite plates*, GTL Report No. 197, MIT, Cambridge, MA (1989).

18. E. K. Dimitriadis, C. R. Fuller and C. A. Rogers, Piezoelectric actuators for distributed noise and vibration excitation of thin plates, in: *Proc. ASME Failure Prevention and Reliability Conf.,* Montreal, pp. 223–233 (1989).
19. B. T. Wang, E. K. Dimitriadis and C. R. Fuller, Active control of panel related noise using multiple piezoelectric actuators, *J. Acoust. Soc. Amer*. **86**, No. S1, S84 (1989).
20. M. C. Ray, R. Bhattacharya and B. Samanta, Exact solutions for static analysis of intelligent structures, *AIAA Journal* **31**, 1684–1691 (1993).
21. P. Heyliger, Static behavior of laminated elastic/piezoelectric plates, *AIAA Journal* **32**, 2481–2488 (1994).
22. K. Y. Sze, X.-M. Yang and H. Fan, Electric assumptions for piezoelectric laminate analysis, *Int. J. Solids Struct*. **41**, 2363–2382 (2004).
23. H. M. Shodja and M. T. Kamali, Three-dimensional analysis of piezocomposite plates with arbitrary geometry and boundary conditions, *Int. J. Solids Struct*. **40**, 4837–4858 (2003).
24. R. M. Jones, *Mechanics of Composite Materials*, Taylor and Francis, Pennsylvania (1999).
25. J. M. Whitney, *Structural Analysis of Laminated Anisotropic Plates*, Technomic Publishing Company, Pennsylvania (1987).
26. K. Michael and I. Hans, On the influence of the electric field on free transverse vibrations of smart beams, *Smart Mater. Struct*. **8**, 401–410 (1999).
27. T.-Y. Zhang, C.-F. Qian and P. Tong, Linear electro-elastic analysis of a cavity or a crack in a piezoelectric material, *Int. J. Solids Struct.* **35**, 2121–2149 (1998).
28. E. Reissner and Y. Stavsky, Bending and stretching of certain types of heterogeneous aeolotropic elastic plates, *J. Appl. Mechan.* **28**, 402–408 (1961).
29. J. Q. Cheng, T.-Y. Zhang, M. H. Zhao, C. F. Qian, S. W. R. Lee and P. Tong, Effects of electric fields on the bending behavior of piezoelectric composite laminates, *Smart Mater. Struct*. **9**, 824–831 (2000).
30. E. Reissner, The effect of transverse shear deformation on the bending of elastic plates, *J. Appl. Mechan*. **12**, 69–77 (1945).
31. R. D. Mindlin, Influence of rotatory inertia and shear on flexural motions of isotropic, elastic plates, *J. Appl. Mechan*. **18**, 336–343 (1951).
32. J. N. Reddy, A generalization of two-dimensional theories of laminated composited plates, *Comm. Appl. Numer. Meth*. **3**, 173–180 (1987).